






Quantal diffusion description of isotope production via the multinucleon transfer mechanism in $^{48}\text{Ca} + ^{238}\text{U}$ collisions

S. Ayik ^{1,*}, M. Arik ², E. C. Karanfil ², O. Yilmaz,² B. Yilmaz ³, and A. S. Umar ⁴

¹*Physics Department, Tennessee Technological University, Cookeville, Tennessee 38505, USA*

²*Physics Department, Middle East Technical University, 06800 Ankara, Turkey*

³*Physics Department, Faculty of Sciences, Ankara University, 06100 Ankara, Turkey*

⁴*Department of Physics and Astronomy, Vanderbilt University, Nashville, Tennessee 37235, USA*



(Received 28 August 2021; accepted 15 November 2021; published 30 November 2021)

As an extension of previous work, we calculate the production cross section of heavy neutron-rich isotopes by employing the quantal diffusion description to $^{48}\text{Ca} + ^{238}\text{U}$ collisions. The quantal diffusion is deduced from stochastic mean-field approach, and transport properties are determined in terms of time-dependent single-particle wave functions of the time-dependent Hartree-Fock theory. As a result, the approach allows for prediction of production cross sections without any adjustable parameters. The secondary cross sections by particle emission are calculated with the help of the statistical GEMINI++ code.

DOI: [10.1103/PhysRevC.104.054614](https://doi.org/10.1103/PhysRevC.104.054614)

I. INTRODUCTION

Extensive experimental investigations of the multinucleon transfer process have been done in heavy-ion collisions with actinide targets at near barrier energies [1–9], and more investigation are currently in progress. These studies may provide an efficient mechanism for production of heavy neutron-rich isotopes, which may not otherwise be possible in fusion, fission, and fragmentation reactions. In quasifission reactions, colliding nuclei stick together in a dinuclear configuration. During long contact times, large number of nucleons are transferred between projectile-like and target-like nuclei.

In theoretical studies of multinucleon transfer mechanism a number of macroscopic models have been employed including the dinuclear system model [10–13], Langevin-type stochastic models [14–19], and the quantum diffusion model [20–22]. These phenomenological models with a number of adjustable parameters provide qualitative and partly semi-quantitative description of the reaction mechanism.

In order to provide a more reliable predictive capability, it is highly desirable to develop a microscopic description without any adjustable parameters. The time-dependent Hartree-Fock (TDHF) theory with effective interactions (effective energy density functional) provides a microscopic description for nuclear dynamics at low energies where the Pauli blocking is very effective [23–27]. The applicability of TDHF to study quasifission for a wide selection of systems is well established [25–34] (see [23,35–37] for recent reviews of TDHF applications to heavy-ion reactions). However, the TDHF theory has a severe limitation: it can only describe the most probable dynamical path of the collision dynamics with

small fluctuations around it. It describes the mean kinetic energy loss due to one body dissipation rather well but it cannot describe the large dispersions of mass and charge distribution of the fragments. Particle projection method applied to TDHF clearly demonstrates that dispersion of a few nucleon transfers are described reasonable well but it falls short for a large number of transfers [31,38]. This suggests that an improvement of the TDHF theory beyond the mean-field approximation is required. The time-dependent random phase approximation of Balian and Vénéroni provided a significant improvement beyond the mean field approximation for the dispersions of the one-body observables [39–42].

The stochastic mean-field (SMF) approach provides further improvement of the TDHF beyond the mean field approximation [43–46]. In particular, the quantal transport description obtained by projecting the SMF approach on a collective space provides a powerful microscopic tool for describing multinucleon transfer mechanism, energy dissipation and fluctuations in low energy heavy-ion collisions. As we discussed in publication [47], employing closure relation in diabatic limit makes it possible to calculate macroscopic transport coefficients in terms of only the occupied single particle states of TDHF. As a result, microscopic transport description of dissipation and fluctuation dynamics of low heavy-ion collisions are characterized in terms of TDHF wave functions by taking quantal effects due to shell structure, full collision geometry and Pauli exclusion principle into account without any adjustable parameters. In the analyses, we do not make a distinction between quasifission and multinucleon transfer mechanism.

In Sec. II we briefly describe the quantal diffusion description of multinucleon transfer based on the SMF approach. Section III presents the result of calculations of isotope cross section produced in $^{48}\text{Ca} + ^{238}\text{U}$ collisions at $E_{c.m.} = 193$ MeV. In Sec. IV, conclusions are given.

* ayik@tntech.edu

II. QUANTUM DIFFUSION DESCRIPTION OF MULTINUCLEON TRANSFER

In TDHF theory a unique single-particle density matrix is calculated with a given initial condition. On the other hand, in the SMF approach to the mean-field theory an ensemble of single-particle density matrices are generated by incorporating the fluctuations of the initial state. The single particle density matrix in each event is determined by the TDHF equations with the self-consistent Hamiltonian of that event. In each event of the SMF approach, fluctuations of the random element of the initial density matrices are determined by Gaussian distributions with variances specified by the requirement that ensemble average of dispersions of one-body observables matches the quantal expressions in the mean-field approach.

When a dinuclear structure is maintained in the collision dynamics, we do not need to generate an ensemble of mean-field events. In this case, it is possible to develop much easier transport description in terms of Langevin transport equations for relevant macroscopic variables by the geometric projection procedure of the SMF approach with the help of the window dynamics. For details of the quantal diffusion description and the window dynamics we refer to Refs. [46–52]. For describing nucleon diffusion mechanism, we consider neutron number and proton number of the projectile-like fragments as relevant macroscopic variables. We can determine the neutron $N_1^\lambda(t)$ and proton $Z_1^\lambda(t)$ numbers of the projectile-fragments in an event λ by integrating the particle density on the left side or the right side of the window, according to the window dynamics,

$$\begin{pmatrix} N_1^\lambda(t) \\ Z_1^\lambda(t) \end{pmatrix} = \int d^3r \Theta[(x - x_0) \cos \theta + (y - y_0) \sin \theta] \times \begin{pmatrix} \rho_n^\lambda(\vec{r}, t) \\ \rho_p^\lambda(\vec{r}, t) \end{pmatrix}, \quad (1)$$

where the quantity

$$\rho_\alpha^\lambda(\vec{r}, t) = \sum_{ij \in \alpha} \Phi_j^{*\alpha}(\vec{r}, t; \lambda) \rho_{ji}^\lambda \Phi_i^\alpha(\vec{r}, t; \lambda) \quad (2)$$

denotes the neutron and proton number ($\alpha = n, p$) densities in the event λ of the ensemble of the single-particle density matrices. In this expression, $x_0(t)$ and $y_0(t)$ are the coordinates of the window center relative to the origin of the center of mass frame, $\theta(t)$ is the smaller angle between the orientation of the symmetry axis of the dinuclear system and the beam direction. Neutron and proton numbers of the projectile-like fragments (or target-like fragments) fluctuate from one event to another, and these numbers can be decomposed as $N_1^\lambda(t) = N_1(t) + \delta N_1^\lambda(t)$ and $Z_1^\lambda(t) = Z_1(t) + \delta Z_1^\lambda(t)$. Here, $N_1(t)$ and $Z_1(t)$ are the mean values determined by the mean-field description of the TDHF theory. According to the quantal diffusion approach, fluctuations of the neutron $\delta N_1^\lambda(t)$ and the proton $\delta Z_1^\lambda(t)$ numbers evolve according to the coupled

Langevin equations

$$\frac{d}{dt} \begin{pmatrix} \delta Z_1(t) \\ \delta N_1(t) \end{pmatrix} = \begin{pmatrix} \frac{\partial v_p}{\partial Z_1} (Z_1^\lambda - Z_1) + \frac{\partial v_p}{\partial N_1} (N_1^\lambda - N_1) \\ \frac{\partial v_n}{\partial Z_1} (Z_1^\lambda - Z_1) + \frac{\partial v_n}{\partial N_1} (N_1^\lambda - N_1) \end{pmatrix} + \begin{pmatrix} \delta v_p^\lambda(t) \\ \delta v_n^\lambda(t) \end{pmatrix}, \quad (3)$$

where quantities $v_\alpha^\lambda(t) = v_\alpha(t) + \delta v_\alpha^\lambda(t)$ are the drift coefficients of neutrons and protons with the mean values and the fluctuating parts are expressed by $v_\alpha(t)$ and $\delta v_\alpha^\lambda(t)$, with α denoting neutron and proton labels. The linear limit of Langevin description presented here provides a good approximation when the driving potential energy is nearly harmonic around the mean values of the mass and charge asymmetry. The mean values of drift coefficients are extracted from TDHF, and their derivatives are evaluated at the mean values. The explicit expressions of the stochastic parts of drift coefficients $\delta v_\alpha^\lambda(t)$ can be found in Ref. [47].

A. Quantal diffusion coefficients

Stochastic part of the drift coefficients, $\delta v_p^\lambda(t)$ and $\delta v_n^\lambda(t)$, provide the source for generating fluctuations in mass and charge asymmetry degrees of freedom. According to the SMF approach, stochastic parts of drift coefficients have Gaussian random distributions with zero mean values, $\delta \bar{v}_p^\lambda(t) = 0$, $\delta \bar{v}_n^\lambda(t) = 0$, and the autocorrelation functions of stochastic drift coefficient integrated over their time history determine diffusion coefficients $D_{\alpha\alpha}(t)$ for proton and neutron transfers,

$$\int_0^t dt' \overline{\delta v_\alpha^\lambda(t) \delta v_\alpha^\lambda(t')} = D_{\alpha\alpha}(t). \quad (4)$$

In general diffusion coefficients involve a complete set of particle-hole states. It is possible to eliminate the entire set of particle states by employing closure relations in the diabatic limit, which is a good approximation for evolution of TDHF wave function during short time intervals. This provides a great simplification and as a result, diffusion coefficients are determined entirely in terms of the occupied single-particle states of the TDHF evolution. Explicit expressions of diffusion coefficients are provided in previous publications [46–51] and for analysis of these coefficients please see Appendix B in Ref. [47]. As seen in these expressions, the source of fluctuations, which are expressed with diffusion coefficient, are specified by the mean-field properties. This result is consistent with the fluctuation dissipation theorem of non-equilibrium statistical mechanics and greatly simplifies calculations of the diffusion coefficient. Diffusion coefficients include the quantal effects due to shell structure, Pauli blocking, and full effect of the collisions geometry without any adjustable parameters. We observe that there is a close analogy between the quantal expression and the classical diffusion coefficient in the random walk problem [53–55]. The direct part is given as the sum of the nucleon currents across the window from the target-like fragment to the projectile-like fragment and from the projectile-like fragment to the target-like fragment, which is integrated over the memory. This is analogous to the random walk problem, in which the diffusion coefficient is given by the sum of the rate for the forward and backward steps. The second part in the quantal diffusion expression stands

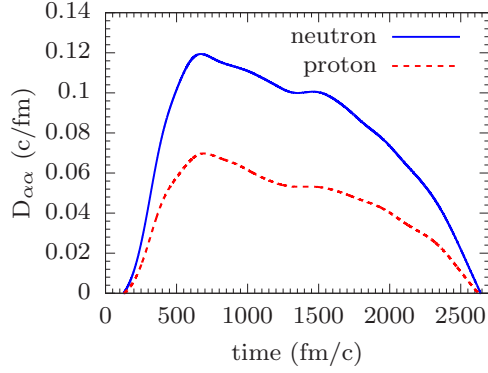


FIG. 1. Neutron and proton diffusion coefficients as a function of time in $^{48}\text{Ca} + ^{238}\text{U}$ collision at $E_{\text{c.m.}} = 193$ MeV for the tip geometry of the uranium and initial orbital angular momentum $\ell = 40\hbar$.

for the Pauli blocking effects in nucleon transfer mechanism, which does not have a classical counterpart. As an example, in Fig. 1 we present neutron and proton diffusion coefficients in $^{48}\text{Ca} + ^{238}\text{U}$ collision at $E_{\text{c.m.}} = 193$ MeV for the initial angular momentum $\ell = 40\hbar$.

B. Derivatives of drift coefficients

To solve the coupled Langevin Eqs. (3) we need to evaluate derivatives of the mean drift coefficients with respect to neutron and proton numbers. A single mean-field event is not sufficient to evaluate these derivatives. To calculate derivatives, one needs to evolve several mean-field events with similar initial conditions. As another possibility for determining the derivatives, we can employ the Einstein relation in the over damped limit [46–51]. In the over damped limit, drift coefficients are related to the driving potential energy surface in (N, Z) plane as

$$\begin{aligned} v_n &= -\frac{D_{NN}}{T^*} \frac{\partial U}{\partial N_1}, \\ v_z &= -\frac{D_{ZZ}}{T^*} \frac{\partial U}{\partial Z_1}, \end{aligned} \quad (5)$$

where T^* and $U(N_1, Z_1)$ represent the effective temperature and the potential energy surface of the system. As an example, Fig. 2 shows the evolution of the mean values of neutron and proton numbers of projectile-like fragments as a function of time in $^{48}\text{Ca} + ^{238}\text{U}$ collision at $E_{\text{c.m.}} = 193$ MeV for the tip orientation with initial orbital angular momentum $\ell = 40\hbar$. The thick black line in Fig. 3 shows the drift path, which represents the mean evolution of neutron and proton numbers of the projectile-like fragments in the (N, Z) plane. The charge asymmetry of projectile ^{48}Ca and target ^{238}U are $(N - Z)/(N + Z) \approx 0.17$ and $(N - Z)/(N + Z) \approx 0.23$, respectively. During the initial phase of the collision from touching point at $t_A = 180$ fm/c until about $t_B = 480$ fm/c system rapidly evolves toward charge equilibration with charge asymmetry approximately equal to $(N - Z)/(N + Z) \approx 0.20$. After this instant the system follows nearly a straight line path, referred to as the iso-scalar path, toward mass symmetry at which neutron and proton numbers

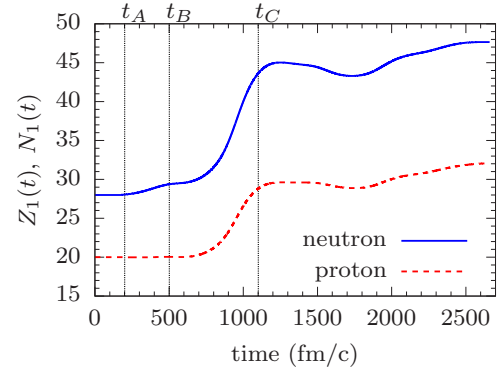


FIG. 2. Mean drift path of the projectile-like fragments in (N, Z) plane for the $^{48}\text{Ca} + ^{238}\text{U}$ collision with tip geometry of the uranium at bombarding energy $E_{\text{c.m.}} = 193$ MeV and initial angular momentum $\ell = 40\hbar$.

are $N_0 = (N_p + N_T)/2 = 87$, $Z_0 = (Z_p + Z_T)/2 = 56$. We approximately describe the potential energy surface of the the system in (N, Z) plane in terms of two parabolas. One of these parabolas is oriented along the isoscalar direction with its minimum located at the mass symmetry point and the second one is oriented in a direction perpendicular to the isoscalar path with its minimum located at the isoscalar path at each point and it is referred to as the isovector path. Potential energy of a fragment with (N_1, Z_1) is approximately given by

$$U(N_1, Z_1) = \frac{1}{2}aR_S^2(N_1, Z_1) + \frac{1}{2}bR_V^2(N_1, Z_1). \quad (6)$$

Here, $R_V = (Z_0 - Z_1) \sin \phi + (N_0 - N_1) \cos \phi$ and $R_S = (Z_0 - Z_1) \cos \phi - (N_0 - N_1) \sin \phi$, represent the distance of a fragment with (N_1, Z_1) from the equilibrium point and the perpendicular distance from the isoscalar path, respectively. The angle ϕ is the angle between the isoscalar path and N axis, which is about $\phi = 32^\circ$. Using Einstein relations in Eq. (5), we can determine the reduced curvature parameters $\alpha = a/T^*$ and $\beta = b/T^*$ in terms of drift and diffusion coefficients. Since only ratios of the curvature parameters (a, b) and the effective temperature appear, the effective temperature is not a parameter in the description. Due to the shell effect the reduced curvature parameters vary in time during the TDHF evolution. We can estimate reduced curvature parameters by

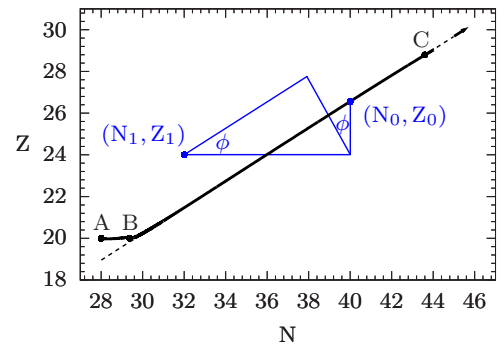


FIG. 3. The mean-drift path in the (N, Z) plane for the $^{48}\text{Ca} + ^{238}\text{U}$ collision with tip geometry of the uranium at bombarding energy $E_{\text{c.m.}} = 193$ MeV and initial angular momentum $\ell = 40\hbar$.

taking average over suitable time intervals. Time interval from touching point A at $t_A = 200$ fm/c until point B at $t_B = 500$ fm/c, where charge asymmetry equilibration is reached, provides a suitable interval for calculating the average value of the reduced isovector curvature parameter,

$$\alpha = 1/(t_B - t_A) \int_{t_A}^{t_B} \left(\frac{v_n(t) \sin \phi}{D_{NN}(t)} - \frac{v_p(t) \cos \phi}{D_{ZZ}(t)} \right) / R_S(t) dt. \quad (7)$$

We can also estimate the reduced isoscalar curvature parameter as average over the time interval from $t_B = 500$ fm/c until close to separation time $t_C = 1200$ fm/c,

$$\beta = 1/(t_B - t_A) \int_{t_B}^{t_C} \left(\frac{v_n(t) \cos \phi}{D_{NN}(t)} + \frac{v_p(t) \sin \phi}{D_{ZZ}(t)} \right) / R_V(t) dt. \quad (8)$$

We deduce average value of the reduced curvature parameters as $\alpha = 0.13$ and $\beta = 0.05$. The potential energy surface has a sharp slope in isovector direction and much shallower in the isoscalar direction. This is a typical behavior of the potential energy surface. In a previous work [47], we have determined the curvature parameters as a function of time for the same system. Here, we evaluate average values of the reduced curvature parameters over the suitable time intervals. In heavy dinuclear systems centrifugal potential energy has a small contribution to the potential energy surface. Therefore, the curvature parameters we estimated for the initial angular momentum $\ell = 40\hbar$ provide a good approximation for the other angular momenta as well. Since the drift coefficients have an analytical form, we can immediately determine their derivatives as

$$\frac{\partial v_n}{\partial N_1} = -D_{NN}(\alpha \sin^2 \phi + \beta \cos^2 \phi), \quad (9)$$

$$\frac{\partial v_z}{\partial Z_1} = -D_{ZZ}(\alpha \cos^2 \phi + \beta \sin^2 \phi), \quad (10)$$

$$\frac{\partial v_n}{\partial Z_1} = -D_{NN}(\beta - \alpha) \sin \phi \cos \phi, \quad (11)$$

$$\frac{\partial v_z}{\partial N_1} = -D_{ZZ}(\beta - \alpha) \sin \phi \cos \phi. \quad (12)$$

The curvature parameter α perpendicular to the β stability valley is much larger than the curvature parameter β along the stability valley. Consequently, β does not have an appreciable effect on the derivatives of the drift coefficients.

C. Fragment probability distributions

In general, joint probability distribution function $P_\ell(N, Z)$ for producing a binary fragment with neutron N and proton Z numbers is determined by generating a large number of solutions of Langevin Eq. (3). It is well known that the Langevin equation is equivalent to the Fokker-Planck equation for the distribution function of the macroscopic variables [55]. In the particular case when drift coefficients are linear functions of macroscopic variables, as we have in Eq. (3), the proton and neutron distribution function for initial angular momentum ℓ is given as a correlated Gaussian function described by the

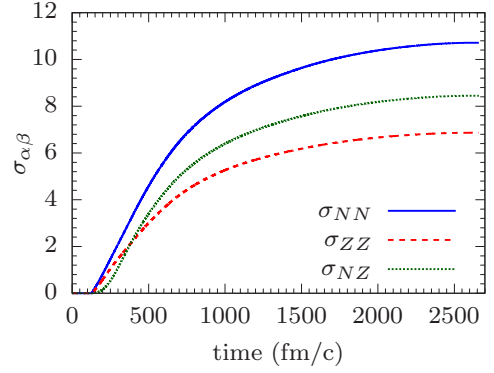


FIG. 4. Neutron, proton, and mixed variances as a function of time in the $^{48}\text{Ca} + ^{238}\text{U}$ collision for the tip geometry of the uranium at bombarding energy $E_{c.m.} = 193$ MeV and initial angular momentum $\ell = 40\hbar$.

mean values, the neutron, proton and, mixed dispersions as

$$P_\ell(N, Z) = \frac{1}{2\pi \sigma_{NN}(\ell) \sigma_{ZZ}(\ell) \sqrt{1 - \rho_\ell^2}} \exp(-C_\ell). \quad (13)$$

Here, the exponent C_ℓ for each impact parameter is given by

$$C_\ell = \frac{1}{2(1 - \rho_\ell^2)} \left[\left(\frac{Z - Z_\ell}{\sigma_{ZZ}(\ell)} \right)^2 - 2\rho_\ell \left(\frac{Z - Z_\ell}{\sigma_{ZZ}(\ell)} \right) \left(\frac{N - N_\ell}{\sigma_{NN}(\ell)} \right) + \left(\frac{N - N_\ell}{\sigma_{NN}(\ell)} \right)^2 \right] \quad (14)$$

with $\rho_\ell = \sigma_{NZ}^2(\ell) / (\sigma_{ZZ}(\ell) \sigma_{NN}(\ell))$. It is possible to deduce coupled differential equations for variances $\sigma_{NN}^2(\ell) = \overline{\delta N^\lambda \delta N^\lambda}$, $\sigma_{ZZ}^2(\ell) = \overline{\delta Z^\lambda \delta Z^\lambda}$, and covariances $\sigma_{NZ}^2(\ell) = \overline{\delta N^\lambda \delta Z^\lambda}$ by multiplying Langevin Eq. (3) by δN^λ and δZ^λ and taking the average over the ensemble generated from the solution of the Langevin equation. These coupled equations are presented in Refs. [47–51]. Variances and covariances are determined from the solutions of these coupled differential equations with initial conditions $\sigma_{NN}^2(t=0) = 0$, $\sigma_{ZZ}^2(t=0) = 0$, and $\sigma_{NZ}^2(t=0) = 0$ for each angular momentum. As an example, Fig. 4 shows neutron, proton, and mixed variances as a function of time for the $^{48}\text{Ca} + ^{238}\text{U}$ collisions in the tip orientation of uranium with the bombarding energy $E_{c.m.} = 193$ MeV for the initial angular momentum $\ell = 40\hbar$. The set of coupled equations are also familiar from the phenomenological nucleon exchange model, and they were derived from the Fokker-Planck equation for the fragment neutron and proton distributions in the deep-inelastic heavy-ion collisions [56,57]. The quantities $N_\ell = \bar{N}_\ell^\lambda$, $Z_\ell = \bar{Z}_\ell^\lambda$ denote the mean neutron and proton numbers of the target-like or project-like fragments. These mean values are determined by the TDHF calculations.

III. RESULTS

In a previous investigation [47], we have calculated primary fragment mass yield in $^{48}\text{Ca} + ^{238}\text{U}$ collisions at bombarding energy $E_{c.m.} = 193$ MeV, and compared the result

TABLE I. Final orbital angular momentum ℓ_f , final average total kinetic energy (TKE), average total excitation energy E^* and scattering angles corresponding to a range of initial angular momentum ℓ_i .

ℓ_i (\hbar)	ℓ_f (\hbar)	TKE	E^*	$\theta_{\text{c.m.}}$	θ_1^{lab}	θ_2^{lab}
38	32.8	203.6	76.1	92.8	77.6	52.7
40	33.4	207.8	78.9	86.8	72.0	57.3
42	33.2	203.8	78.4	85.3	70.6	57.8
44	34.7	206.4	69.4	91.5	76.6	53.6
46	38.6	197.7	71.6	91.5	52.4	75.0
48	38.0	195.6	77.6	88.9	74.0	54.1
50	39.8	197.2	74.6	86.9	72.1	55.6
52	42.8	199.5	72.2	85.3	70.7	56.9
54	43.6	196.2	73.0	84.1	69.7	57.1
56	44.2	187.7	81.5	83.5	68.9	56.6

with experimental data of Kozulin *et al.* [2]. Here, we present results for cross sections $\sigma(N, Z)$ of production of primary and secondary isotopes with proton numbers $Z = 64\text{--}80$ in the same system at the same bombarding energy. Also we improve the yield calculation by including binary fragment production by fusion-fission mechanism. We assume the same experimental set up where the detectors are placed at angles $\pm 64^\circ$ with 10° acceptance range in laboratory frame. We consider three collision geometries of the target nucleus: tip configuration where the symmetry axis of uranium is parallel to the beam direction and two side geometries in which symmetry axis of uranium perpendicular to the beam direction (in reaction plane and perpendicular to reaction plane). According to the TDHF calculations, mean trajectories of fragments reach the acceptance range of detectors in collisions only in the tip configuration with initial angular momentum in the range $\ell = 38\text{--}56\hbar$. Table I shows results of TDHF calculations in tip geometry for final angular momentum, final total kinetic energy, total excitation energy, scattering angles in the center of mass frame and laboratory frame for a range initial angular momentum. The results presented in this table are obtained by performing calculations with the TDHF code [58]. According to the detector set up, the range of initial angular momentum $\ell = 38\text{--}56\hbar$ is within the acceptance range of detectors. Table II shows the mean values of initial and final

 TABLE II. Mean values of mass and charge numbers of the initial and final fragments, neutron variance, proton variance, and mixed variance for a range of initial orbital angular momentum ℓ_i .

ℓ_i (\hbar)	A_1^f	Z_1^f	A_2^f	Z_2^f	σ_{NN}^2	σ_{ZZ}^2	σ_{NZ}^2	σ_{AA}^2
38	78.5	31.5	207.5	80.5	115.7	50.5	67.8	234.0
40	79.7	32.1	206.3	79.9	116.8	50.9	68.6	236.3
42	78.6	31.6	207.4	80.4	114.6	49.9	67.1	231.6
44	77.5	31.2	208.5	80.8	107.2	46.8	62.3	216.3
46	75.0	30.1	211.0	81.9	102.4	44.8	59.2	206.4
48	75.8	30.5	210.2	81.5	101.6	44.4	58.6	204.6
50	76.1	30.6	209.9	81.4	99.8	43.7	57.5	201.0
52	76.3	30.8	209.7	81.3	97.4	42.7	55.9	196.0
54	75.2	30.3	210.8	81.7	94.5	41.4	54.0	189.9
56	74.2	30.1	211.8	81.9	91.6	40.2	52.1	183.9

mass and charge numbers of projectile-like and target-like fragments. Same table shows asymptotic values of quantum diffusion calculations for neutron σ_{NN}^2 , proton σ_{ZZ}^2 , and mixed σ_{NZ}^2 variances. Since we determine curvature parameters of the potential energy using a different approach, some differences appear for dispersion results from those presented in [47].

A. Primary mass yield

In the previous investigation, we included only the multi-nucleon transfer (mnt) processes in the primary yield calculations. Here, we improve the yield calculations by incorporating binary fragments production in fusion-fission (ff) processes. We can express the yield of primary fragments mass distribution according to

$$Y(A) = \eta(P^{\text{mnt}}(A) + P^{\text{ff}}(A)), \quad (15)$$

where $P^{\text{mnt}}(A)$ and $P^{\text{ff}}(A)$ are the fragment mass distributions due to multi-nucleon transfer and due to fusion-fission mechanism, respectively, and η is a normalization constant. According to quantal diffusion calculations, probability distribution due to multinucleon transfer is given by

$$P(A) = \frac{1}{\sum_{\ell} (2\ell + 1)} \sum_{\ell} (2\ell + 1) [P_{\ell}^{\text{pro}}(A) + P_{\ell}^{\text{tar}}(A)] \quad (16)$$

with the range of initial angular momentum spanning the interval $\ell = 38\text{--}56\hbar$. Here, $P_{\ell}^{\text{pro}}(A)$ and $P_{\ell}^{\text{tar}}(A)$ are mass distributions of projectile-like and target-like fragments. We can determine the probability distribution $P_{\ell}(A)$ of the mass number A of the primary fragments, by integrating Eq. (16) over Z substituting $N = A - Z$ to find

$$P_{\ell}^{\ell}(A) = \frac{1}{\sqrt{2\pi}\sigma_{AA}} \exp\left\{-\frac{1}{2}\left[\frac{(A - A_{\ell})}{\sigma_{AA}(\ell)}\right]^2\right\}. \quad (17)$$

Here, mass dispersion is given by $\sigma_{AA}^2 = \sigma_{NN}^2 + \sigma_{ZZ}^2 + 2\sigma_{NZ}^2$ and A_{ℓ} indicates the mean value of the mass number projectile-like or target-like for each angular momentum. We cannot employ quantal diffusion approach to determine fragment mass distribution due to fusion-fission mechanism. However we can estimate fusion-fission probability in the following manner: Bombarding energy $E_{\text{c.m.}} = 193.1$ MeV is very close to fusion barrier located around $E_{\text{bar}} = 193.8$ MeV. At this bombarding energy, TDHF calculations are not very reliable for determining fusion probability. We assume that at this bombarding energy near central collisions up to critical angular momentum ℓ_c lead to fusion. The excitation energy of the compound nucleus is determined as $E_C^* = E_{\text{c.m.}} - Q_{\text{gg}}$, where Q_{gg} is the ground state Q value of the compound nucleus relative to the initial state. We determine fission probability compound nucleus into binary fragments using GEMINI++ code [59]. Normalized mass distribution of binary fragments is given by

$$P^{\text{ff}}(A) = \frac{1}{\sum_{\ell} (2\ell + 1)} \sum_{\ell} (2\ell + 1) P_{\ell}^{\text{ff}}(A). \quad (18)$$

Here, $P_{\ell}^{\text{ff}}(A)$ denotes fission probability distribution of the compound nucleus produced in collision with initial angular

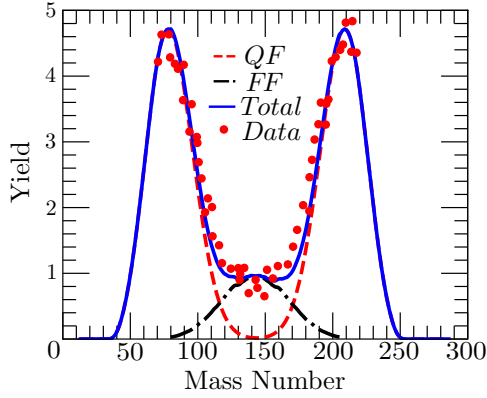


FIG. 5. Solid blue line shows the combined primary yield of multi-nucleon transfer (dashed red line in center region) and binary fission (black dashed dotted line) as function fragment mass A in collision of $^{48}\text{Ca} + ^{238}\text{U}$ at $E_{\text{c.m.}} = 193.1$ MeV. Red solid points show data taken from [1].

momentum ℓ . Summation interval extends up to a critical angular momentum $\ell = 0 - \ell_c$. We expect that average value of fission fragment distribution not to be very sensitive to the magnitude of the critical angular momentum. Hence, in calculations we take the critical angular momentum for leading to fusion as $\ell_c = 5\hbar$. In Fig. 5 solid blue line shows the combined primary yield of multinucleon transfer (dashed blue line in center region) and binary fission (blue dashed dotted line) as function of fragment mass. Calculations are compared with data of reference [1] shown by red solid points. Normalization constant in Eq. (15) is determined by fitting data at a suitable point to give $\eta = 214$.

B. Isotope production with $Z = 64-80$

We calculate the cross sections for production of primary isotopes using the standard expression

$$\sigma(N, Z) = \frac{\pi \hbar^2}{2\mu E_{\text{c.m.}}} \sum_{\ell} (2\ell + 1) [P_{\ell}^{\text{pro}}(N, Z) + P_{\ell}^{\text{tar}}(N, Z)]. \quad (19)$$

Here, $P_{\ell}^{\text{pro}}(N, Z)$ and $P_{\ell}^{\text{tar}}(N, Z)$ denote the probability of producing projectile-like and target-like fragments. These probabilities are given by Eq. (13) with mean values of projectile-like and target-like fragments, respectively. In the summation over ℓ , the range of initial angular momentum depends on the detector geometry in the laboratory frame. In calculations we take the range of angular momentum $\ell = 38-56\hbar$ according to the experimental set up of Kozulin *et al.* [2], for the $^{48}\text{Ca} + ^{238}\text{U}$ system at bombarding energy $E_{\text{c.m.}} = 193.1$ MeV. Blue solid lines in Fig. 6 show the production cross sections of primary target-like isotopes with proton number $Z = 65-80$ as a function of mass number A . These primary isotopes are excited and cool down by emitting light particles, mostly neutrons, protons, and α particles, and may also decay via binary fission. In a recent publication [45], employing Eq. (19), we analyzed primary and secondary cross sections for heavy

isotope production in $^{136}\text{Xe} + ^{208}\text{Pb}$ collisions at $E_{\text{c.m.}} = 514$ MeV and compared the results with data reported in the study of Kozulin *et al.* [1]. In that work, we have determined the secondary cross sections by shifting the primary cross sections according to the number of neutrons emitted which is the dominant process in de-excitation mechanism. We estimated the number of emitted neutrons according to the mean excitation energies in heavy primary fragments. In the present study, we determine the secondary cross sections by analyzing de-excitation mechanism of primary fragments using statistical code GEMINI++ [59]. We estimate the total excitation energy of binary primary fragments according to $E_{\ell}^*(Z, A) = E_{\text{c.m.}} - \text{TKE}_{\ell} - Q_{\text{gg}}(Z, A)$. In this expression TKE_{ℓ} is the mean value of total asymptotic kinetic energy in collision with initial angular momentum ℓ and $Q_{\text{gg}}(Z, A)$ denotes ground state Q value of the primary binary fragments relative to the initial value. It is possible to add Coulomb correction to the total final kinetic energy due to proton transfer in excess of the mean number of proton transfer [50]. We ignore this correction in the present study. We share the total excitation energy and total angular momentum transfer in proportion to the mass ratio of binary primary fragments. Red histograms in Fig. 6 show the secondary cross sections for target-like isotopes with proton numbers $Z = 65-80$ as a function of mass number A . We note that secondary isotope distributions shift toward the valley of stability by emitting 5–6 neutrons depending on excitation energy of primary fragments. The secondary cross sections are not obtained from the primary cross sections by merely shifting the primary cross sections with the number of emitted neutrons. According to the statistical de-excitation code GEMINI++, in addition to neutron emission, the secondary isotopes with small proton numbers are populated by de-excitation of primary fragments with larger proton numbers by emitting α particles and protons, and by induced secondary fission. The de-excitation mechanisms other than neutron emission increase the secondary cross sections to the left of peak values of the primary cross sections, and even overshoot the maximum value of the primary cross-sections values as seen in Fig. 6. We also note production cross sections for heavy neutron rich isotopes of mercury, gold and platinum with neutron numbers around 125–130 are in the order of several μb . These cross sections are much larger than the estimates given by Adamian *et al.* [12].

IV. CONCLUSIONS

As an extension of previous work, we have investigated multinucleon transfer mechanism in $^{48}\text{Ca} + ^{238}\text{U}$ collisions at $E_{\text{c.m.}} = 193.1$ MeV using quantal diffusion description based on the SMF approach. In this approach, transport coefficients associated with macroscopic variables such as charge and mass asymmetry variables are evaluated in terms of time-dependent single-particle wave functions of TDHF theory. Transport description includes quantal effects due to shell structure, full geometry of the collision dynamics, and the Pauli exclusion principle without any adjustable parameters aside from the standard description of the effective Hamiltonian of TDHF theory. Joint probability distribution of primary

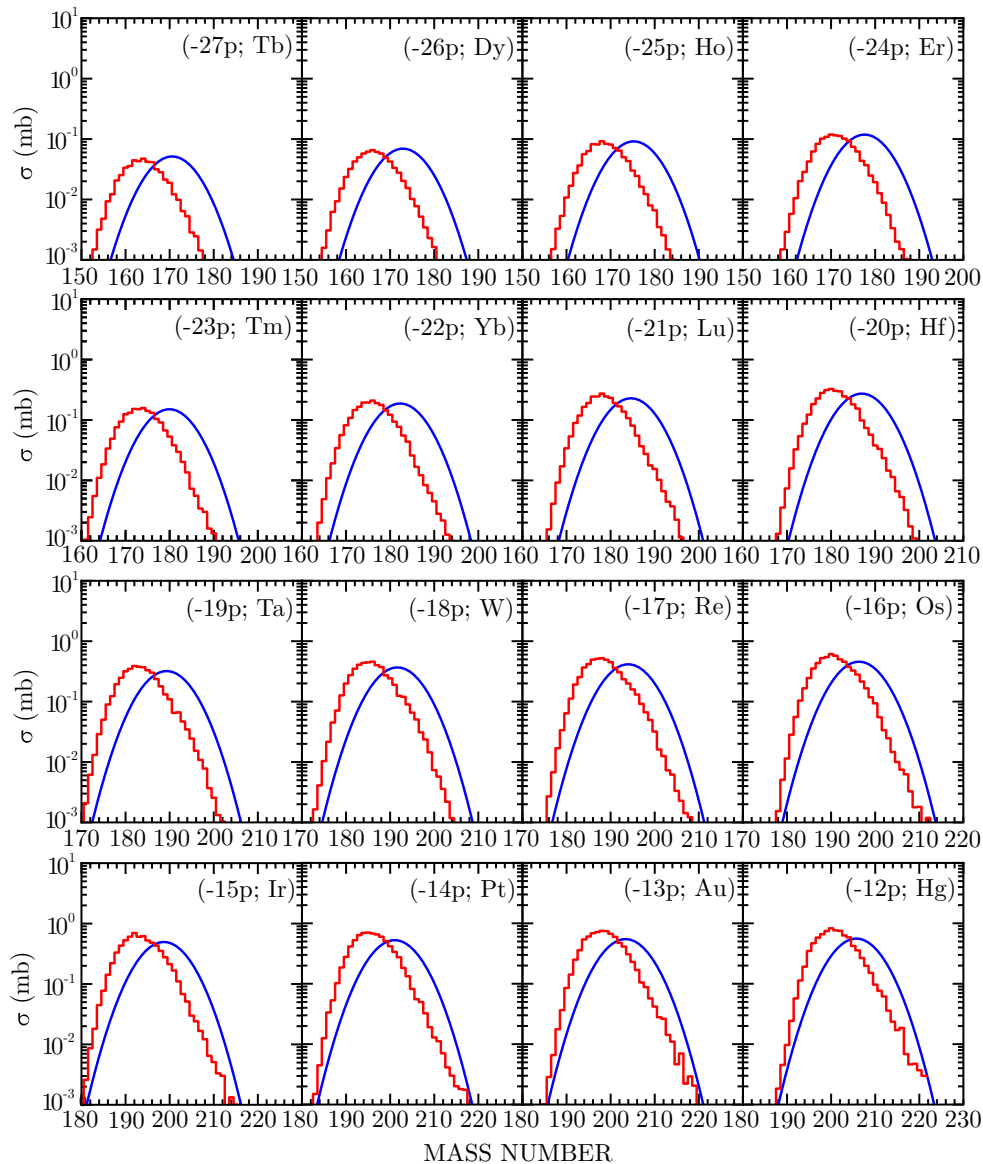


FIG. 6. Solid blue lines show primary isotope yields for $Z = 65-80$ as function fragment mass A in collision of $^{48}\text{Ca} + ^{238}\text{U}$ at $E_{\text{c.m.}} = 193.1$ MeV. Red histograms show production cross-sections of secondary isotopes calculated with GEMINI++ .

fragments is determined by a correlated Gaussian function in terms of mean values of neutron-proton numbers and neutron, proton, mixed dispersions for each initial angular momentum. We calculate the yield of primary fragments as a function of mass number and compare with data of Kozulin *et al.* Primary yield contains fragments produced by multi-nucleon transfer and also secondary fission products. Since the bombarding energy is very close to fusion barrier located at about $E_{\text{bar}} = 193.8$ MeV, TDHF is not very reliable for determining the fusion mechanism. We assume $^{48}\text{Ca} + ^{238}\text{U}$ collisions lead to fission at near central collisions and determine fission probability employing the GEMINI++ code. Calculations produce good description of experimental mass yield distribution. We investigate de-excitation mechanism of heavy target-like primary fragments in the range of

$Z = 65-80$, and calculate secondary isotope cross sections as a function of mass number. Calculations predict cross-sections on the order of several μb for heavy neutron rich isotopes of mercury, gold and platinum with neutron numbers in the range of 125–130.

ACKNOWLEDGMENTS

Authors are thankful to K. Sekizawa for useful discussion on the GEMINI++ code. S.A. gratefully acknowledges Middle East Technical University for warm hospitality extended to him during his visits. S.A. also gratefully acknowledges F. Ayik for continuous support and encouragement. This work is supported in part by US DOE Grant No. DE-SC0015513, and in part by US DOE Grant No. DE-SC0013847.

- [1] E. M. Kozulin, E. Vardaci, G. N. Knyazheva, A. A. Bogachev, S. N. Dmitriev, I. M. Itkis, M. G. Itkis, A. G. Knyazev, T. A. Loktev, K. V. Novikov, E. A. Razinkov, O. V. Rudakov, S. V. Smirnov, W. Trzaska, and V. I. Zagrebaev, Mass distributions of the system $^{136}\text{Xe} + ^{208}\text{Pb}$ at laboratory energies around the Coulomb barrier: A candidate reaction for the production of neutron-rich nuclei at $N = 126$, *Phys. Rev. C* **86**, 044611 (2012).
- [2] E. M. Kozulin, G. N. Knyazheva, I. M. Itkis, N. I. Kozulina, T. A. Loktev, K. V. Novikov, and I. Harca, Shell effects in fission, quasifission and multinucleon transfer reaction, *J. Phys.: Conf. Ser.* **515**, 012010 (2014).
- [3] J. V. Kratz, M. Schädel, and H. W. Gäggeler, Reexamining the heavy-ion reactions $^{238}\text{U} + ^{238}\text{U}$ and $^{238}\text{U} + ^{248}\text{Cm}$ and actinide production close to the barrier, *Phys. Rev. C* **88**, 054615 (2013).
- [4] Y. X. Watanabe, Y. H. Kim, S. C. Jeong, Y. Hirayama, N. Imai, H. Ishiyama, H. S. Jung, H. Miyatake, S. Choi, J. S. Song, E. Clement, G. de France, A. Navin, M. Rejmund, C. Schmitt, G. Pollarolo, L. Corradi, E. Fioretto, D. Montanari, M. Niikura *et al.*, Pathway for the production of neutron-rich isotopes around the $N = 126$ shell closure, *Phys. Rev. Lett.* **115**, 172503 (2015).
- [5] H. M. Devaraja, S. Heinz, O. Beliuskina, V. Comas, S. Hofmann, C. Hornung, G. Münzenberg, K. Nishio, D. Ackermann, Y. K. Gambhir, M. Gupta, R. A. Henderson, F. P. Heßberger, J. Khuyagbaatar, B. Kindler, B. Lommel, K. J. Moody, J. Maurer, R. Mann, A. G. Popeko *et al.*, Observation of new neutron-deficient isotopes with $Z \geq 92$ in multinucleon transfer reactions, *Phys. Lett. B* **748**, 199 (2015).
- [6] V. V. Desai, W. Loveland, K. McCaleb, R. Yanez, G. Lane, S. S. Hota, M. W. Reed, H. Watanabe, S. Zhu, K. Auranen, A. D. Ayangeakaa, M. P. Carpenter, J. P. Greene, F. G. Kondev, D. Seweryniak, R. V. F. Janssens, and P. A. Copp, The $^{136}\text{Xe} + ^{198}\text{Pt}$ reaction: A test of models of multi-nucleon transfer reactions, *Phys. Rev. C* **99**, 044604 (2019).
- [7] B. Birkenbach, A. Vogt, K. Geibel, F. Recchia, P. Reiter, J. J. Valiente-Dobón, D. Bazzacco, M. Bowry, A. Bracco, B. Bruyneel, L. Corradi, F. C. L. Crespi, G. de Angelis, P. Désesquelles, J. Eberth, E. Farnea, E. Fioretto, A. Gadea, A. Gengelbach, A. Giaz *et al.*, Spectroscopy of the neutron-rich actinide nucleus ^{240}U following multinucleon-transfer reactions, *Phys. Rev. C* **92**, 044319 (2015).
- [8] A. Vogt, B. Birkenbach, P. Reiter, L. Corradi, T. Mijatović, D. Montanari, S. Szilner, D. Bazzacco, M. Bowry, A. Bracco, B. Bruyneel, F. C. L. Crespi, G. de Angelis, P. Désesquelles, J. Eberth, E. Farnea, E. Fioretto, A. Gadea, K. Geibel, A. Gengelbach *et al.*, Light and heavy transfer products in $^{136}\text{Xe} + ^{238}\text{U}$ multinucleon transfer reactions, *Phys. Rev. C* **92**, 024619 (2015).
- [9] F. Galtarossa, L. Corradi, S. Szilner, E. Fioretto, G. Pollarolo, T. Mijatović, D. Montanari, D. Ackermann, D. Bourgin, S. Courtin, G. Fruet, A. Goasduff, J. Grebosz, F. Haas, D. Jelavić Malenica, S. C. Jeong, H. M. Jia, P. R. John, D. Mengoni, M. Milin *et al.*, Mass correlation between light and heavy reaction products in multinucleon transfer $^{197}\text{Au} + ^{130}\text{Te}$ collisions, *Phys. Rev. C* **97**, 054606 (2018).
- [10] G. G. Adamian, N. V. Antonenko, and W. Scheid, Characteristics of quasifission products within the dinuclear system model, *Phys. Rev. C* **68**, 034601 (2003).
- [11] G. G. Adamian, N. V. Antonenko, V. V. Sargsyan, and W. Scheid, Possibility of production of neutron-rich Zn and Ge isotopes in multinucleon transfer reactions at low energies, *Phys. Rev. C* **81**, 024604 (2010).
- [12] G. G. Adamian, N. V. Antonenko, V. V. Sargsyan, and W. Scheid, Predicted yields of new neutron-rich isotopes of nuclei with $Z = 64-80$ in the multinucleon transfer reaction $^{48}\text{Ca} + ^{238}\text{U}$, *Phys. Rev. C* **81**, 057602 (2010).
- [13] G. Adamian, N. Antonenko, and W. Scheid, Clustering Effects Within the Dinuclear Model, in *Clusters in Nuclei, Vol. 2*, Lecture Notes in Physics, edited by C. Beck (Springer, Berlin/Heidelberg, 2012), Vol. 848, pp. 165–227.
- [14] Valery Zagrebaev and Walter Greiner, Production of new heavy isotopes in low-energy multinucleon transfer reactions, *Phys. Rev. Lett.* **101**, 122701 (2008).
- [15] V. I. Zagrebaev and W. Greiner, Production of heavy and super-heavy neutron-rich nuclei in transfer reactions, *Phys. Rev. C* **83**, 044618 (2011).
- [16] V. Zagrebaev and W. Greiner, Giant Nuclear Systems of Molecular Type, in *Clusters in Nuclei: Vol. 1*, Lecture Notes in Physics, edited by C. Beck (Springer, Berlin/Heidelberg, 2010), Vol. 818, pp. 267–315.
- [17] V. I. Zagrebaev, A. V. Karpov, and W. Greiner, Possibilities for synthesis of new isotopes of superheavy elements in fusion reactions, *Phys. Rev. C* **85**, 014608 (2012).
- [18] A. V. Karpov and V. V. Saiko, Modeling near-barrier collisions of heavy ions based on a Langevin-type approach, *Phys. Rev. C* **96**, 024618 (2017).
- [19] V. V. Saiko and A. V. Karpov, Analysis of multinucleon transfer reactions with spherical and statically deformed nuclei using a Langevin-type approach, *Phys. Rev. C* **99**, 014613 (2019).
- [20] V. V. Sargsyan, G. G. Adamian, N. V. Antonenko, and W. Scheid, Peculiarities of the sub-barrier fusion with the quantum diffusion approach, *Eur. Phys. J. A* **45**, 125 (2010).
- [21] V. V. Sargsyan, G. G. Adamian, N. V. Antonenko, W. Scheid, and H. Q. Zhang, Role of neutron transfer in capture processes at sub-barrier energies, *Phys. Rev. C* **85**, 024616 (2012).
- [22] V. V. Sargsyan, G. Scamps, G. G. Adamian, N. V. Antonenko, D. Lacroix, W. Scheid, and H. Q. Zhang, Nuclear reactions at near-barrier energies with quantum diffusion approach, *J. Phys.: Conf. Ser.* **515**, 012001 (2014).
- [23] C. Simenel, Nuclear quantum many-body dynamics, *Eur. Phys. J. A* **48**, 152 (2012).
- [24] T. Nakatsukasa, K. Matsuyanagi, M. Matsuo, and K. Yabana, Time-dependent density-functional description of nuclear dynamics, *Rev. Mod. Phys.* **88**, 045004 (2016).
- [25] V. E. Oberacker, A. S. Umar, and C. Simenel, Dissipative dynamics in quasifission, *Phys. Rev. C* **90**, 054605 (2014).
- [26] A. S. Umar, V. E. Oberacker, and C. Simenel, Shape evolution and collective dynamics of quasifission in the time-dependent Hartree-Fock approach, *Phys. Rev. C* **92**, 024621 (2015).
- [27] C. Simenel, K. Godbey, and A. S. Umar, Timescales of quantum equilibration, dissipation and fluctuation in nuclear collisions, *Phys. Rev. Lett.* **124**, 212504 (2020).
- [28] A. Wakhle, C. Simenel, D. J. Hinde, M. Dasgupta, M. Evers, D. H. Luong, R. du Rietz, and E. Williams, Interplay between quantum shells and orientation in quasifission, *Phys. Rev. Lett.* **113**, 182502 (2014).
- [29] K. Hammerton, Z. Kohley, D. J. Hinde, M. Dasgupta, A. Wakhle, E. Williams, V. E. Oberacker, A. S. Umar, I. P. Carter, K. J. Cook, J. Greene, D. Y. Jeung, D. H. Luong, S. D. McNeil, C. S. Palshetkar, D. C. Rafferty, C. Simenel, and K. Stiefel, Reduced quasifission competition in fusion reactions forming

- neutron-rich heavy elements, *Phys. Rev. C* **91**, 041602(R) (2015).
- [30] A. S. Umar, V. E. Oberacker, and C. Simenel, Fusion and quasifission dynamics in the reactions $^{48}\text{Ca} + ^{249}\text{Bk}$ and $^{50}\text{Ti} + ^{249}\text{Bk}$ using a time-dependent Hartree-Fock approach, *Phys. Rev. C* **94**, 024605 (2016).
- [31] K. Sekizawa and K. Yabana, Time-dependent Hartree-Fock calculations for multinucleon transfer and quasifission processes in the $^{64}\text{Ni} + ^{238}\text{U}$ reaction, *Phys. Rev. C* **93**, 054616 (2016).
- [32] L. Guo, C. Shen, C. Yu, and Z. Wu, Isotopic trends of quasifission and fusion-fission in the reactions $^{48}\text{Ca} + ^{239,244}\text{Pu}$, *Phys. Rev. C* **98**, 064609 (2018).
- [33] H. Zheng, S. Burrello, M. Colonna, D. Lacroix, and G. Scamps, Connecting the nuclear equation of state to the interplay between fusion and quasifission processes in low-energy nuclear reactions, *Phys. Rev. C* **98**, 024622 (2018).
- [34] K. Godbey, A. S. Umar, and C. Simenel, Deformed shell effects in $^{48}\text{Ca} + ^{249}\text{Bk}$ quasifission fragments, *Phys. Rev. C* **100**, 024610 (2019).
- [35] C. Simenel and A. S. Umar, Heavy-ion collisions and fission dynamics with the time-dependent Hartree-Fock theory and its extensions, *Prog. Part. Nucl. Phys.* **103**, 19 (2018).
- [36] Kazuyuki Sekizawa, TDHF theory and its extensions for the multinucleon transfer reaction: A mini review, *Front. Phys.* **7**, 20 (2019).
- [37] P. D. Stevenson and M. C. Barton, Low-energy heavy-ion reactions and the Skyrme effective interaction, *Prog. Part. Nucl. Phys.* **104**, 142 (2019).
- [38] C. Simenel, Particle transfer reactions with the time-dependent Hartree-Fock theory using a particle number projection technique, *Phys. Rev. Lett.* **105**, 192701 (2010).
- [39] R. Balian and M. Vénéroni, Time-dependent variational principle for the expectation value of an observable: Mean-field applications, *Ann. Phys. (NY)* **164**, 334 (1985).
- [40] C. Simenel, From Light to Hyper-heavy Molecules and Neutron-Star Crusts in a Dynamical Mean-Field Approach, in *Clusters in Nuclei, Vol. 3*, Lecture Notes in Physics, edited by C. Beck (Springer, Berlin/Heidelberg, 2014), Vol. 875, pp. 95–145.
- [41] E. Williams, K. Sekizawa, D. J. Hinde, C. Simenel, M. Dasgupta, I. P. Carter, K. J. Cook, D. Y. Jeung, S. D. McNeil, C. S. Palshetkar, D. C. Rafferty, K. Ramachandran, and A. Wakhle, Exploring zeptosecond quantum equilibration dynamics: From deep-inelastic to fusion-fission outcomes in $^{58}\text{Ni} + ^{60}\text{Ni}$ reactions, *Phys. Rev. Lett.* **120**, 022501 (2018).
- [42] K. Godbey and A. S. Umar, Quasifission dynamics in microscopic theories, *Front. Phys.* **8**, 40 (2020).
- [43] S. Ayik, A stochastic mean-field approach for nuclear dynamics, *Phys. Lett. B* **658**, 174 (2008).
- [44] D. Lacroix and S. Ayik, Stochastic quantum dynamics beyond mean field, *Eur. Phys. J. A* **50**, 95 (2014).
- [45] S. Ayik, O. Yilmaz, B. Yilmaz, and A. S. Umar, Heavy-isotope production in $^{136}\text{Xe} + ^{208}\text{Pb}$ collisions at $E_{\text{c.m.}} = 514$ MeV, *Phys. Rev. C* **100**, 044614 (2019).
- [46] S. Ayik, B. Yilmaz, O. Yilmaz, A. S. Umar, and G. Turan, Multinucleon transfer in central collisions of $^{238}\text{U} + ^{238}\text{U}$, *Phys. Rev. C* **96**, 024611 (2017).
- [47] S. Ayik, B. Yilmaz, O. Yilmaz, and A. S. Umar, Quantal diffusion description of multinucleon transfers in heavy-ion collisions, *Phys. Rev. C* **97**, 054618 (2018).
- [48] B. Yilmaz, S. Ayik, O. Yilmaz, and A. S. Umar, Multinucleon transfer in $^{58}\text{Ni} + ^{60}\text{Ni}$ and $^{60}\text{Ni} + ^{60}\text{Ni}$ in a stochastic mean-field approach, *Phys. Rev. C* **98**, 034604 (2018).
- [49] S. Ayik, B. Yilmaz, O. Yilmaz, and A. S. Umar, Quantal diffusion approach for multinucleon transfers in Xe+ Pb collisions, *Phys. Rev. C* **100**, 014609 (2019).
- [50] K. Sekizawa and S. Ayik, Quantal diffusion approach for multinucleon transfer processes in the $^{58,64}\text{Ni} + ^{208}\text{Pb}$ reactions: Toward the production of unknown neutron-rich nuclei, *Phys. Rev. C* **102**, 014620 (2020).
- [51] S. Ayik, B. Yilmaz, O. Yilmaz, and A. S. Umar, Merging of transport theory with the time-dependent Hartree-Fock approach: Multinucleon transfer in U + U collisions, *Phys. Rev. C* **102**, 024619 (2020).
- [52] O. Yilmaz, G. Turan, and B. Yilmaz, Quasi-fission and fusion-fission reactions in $^{48}\text{Ca} + ^{208}\text{Pb}$ collisions at $E_{\text{c.m.}} = 190$ MeV, *Eur. Phys. J. A* **56**, 37 (2020).
- [53] C. W. Gardiner, *Quantum Noise* (Springer-Verlag, Berlin, 1991).
- [54] U. Weiss, *Quantum Dissipative Systems*, 2nd ed. (World Scientific, Singapore, 1999).
- [55] Hannes Risken and Till Frank, *The Fokker-Planck Equation* (Springer-Verlag, Berlin, 1996).
- [56] W. U. Schröder, J. R. Huizenga, and J. Randrup, Correlated mass and charge transport induced by statistical nucleon exchange in damped nuclear reactions, *Phys. Lett. B* **98**, 355 (1981).
- [57] A. C. Merchant and W. Nörenberg, Microscopic transport theory of heavy-ion collisions, *Z. Phys. A* **308**, 315 (1982).
- [58] A. S. Umar and V. E. Oberacker, Three-dimensional unrestricted time-dependent Hartree-Fock fusion calculations using the full Skyrme interaction, *Phys. Rev. C* **73**, 054607 (2006).
- [59] R. Charity, GEMINI a code to simulate the decay of a compound nucleus by a series of binary decays, Technical Report No. INDC(NDS)0530, International Atomic Energy Agency (IAEA), 2008.